

Flux-flow in multiband $\text{FeSe}_x\text{Te}_{1-x}$ explored by microwave magnetotransport

A. Magalotti^{1,2}, A. Alimenti^{1,2}, V. Braccini³, P. Manfrinetti⁴, E. Silva^{1,2}, K. Torokhtii¹, N. Pompeo^{1,2}

¹Department of Industrial, Electronic and Mechanical Engineering, Università Roma Tre, Via Vito Volterra 62, 00146 Roma, Italy

²INFN, Roma Tre Section, 00146 Roma, Italy

³CNR-SPIN, Corso Perrone 24, 16152 Genova, Italy

⁴Department of Chemistry and Industrial Chemistry, Università Degli Studi di Genova, Via Dodecaneso 31, 16146 Genova, Italy

E-mail: nicola.pompeo@uniroma3.it

September 4, 2025

Abstract. We measure the flux-flow resistivity in $\text{FeSe}_x\text{Te}_{1-x}$ epitaxial films using a microwave, dual-frequency technique. The flux-flow resistivity allows to open a window on the microscopic electronic state of quasiparticles. We obtain that the field-dependence of flux-flow is typical for multiband superconductors. Once this is assessed, we are able to extract the temperature dependence of the orbital upper critical field and of the normalised vortex core quasiparticle scattering time. Our data suggest that our epitaxial $\text{FeSe}_x\text{Te}_{1-x}$ films are in the moderately clean regime.

Keywords: FeSeTe, microwaves, multiband superconductivity, flux flow resistivity, orbital upper critical field, vortex cores quasiparticle scattering time

1. Introduction

Iron based superconductors (IBS) are well known to be multiband superconductors. Various pairing symmetries are proposed and have found experimental support, typically with more or less anisotropic s-wave gap with possible ++ peculiarities [1]. The Fermi surfaces involves typically two or more bands, with both types of charge carriers (holes and electrons). Moreover, anisotropy is a typical feature of IBS, albeit less prominent than in their cuprate high- T_c cousins.

In the mixed state, vortex structure and dynamics is expected to be deeply impacted by this complex electronic structure, leading for example to fractional vortices, related to the distinct superfluids, which can be locked [2] or lead to dissociate at high driving currents [3]. The multiband nature can also appear in terms of enhanced dissipation at low fields, whenever one of the bands is more strongly depressed by the applied magnetic field, similarly to what happens in MgB_2 [4, 2]. Indeed, the important parameter in this context, the slope α of the normalized flux flow resistivity ρ_{ff}/ρ_n vs the normalized applied magnetic field B/B_{c2} , $\rho_{ff}/\rho_n = \alpha B/B_{c2}$, is expected and observed to be > 1 (ρ_n and B_{c2} are the normal state resistivity and upper critical field, respectively) [5, 6, 7, 8, 9], in contrast with the well-known Bardeen-Stephen behaviour [10] or with more refined results based on Time-Dependent Ginzburg Landau theory [11, 12], although FeSeTe single crystals have exhibited contrasting behaviours [13].

Further complexities arise when the quantization of the bound levels in the vortex cores is investigated, with the possible emergence of the superclean regime: in single-band superconductors the quantitative values of ρ_{ff} can be used as a marker of the superclean/clean regime [14]. However in multiband superconductors the mixing of the bands contributions, with the addition of partial cancelling effects [15] whenever charge carriers of opposite signs are involved, leads to values for ρ_{ff} nominally pertaining to moderately clean regime even in systems like FeSe where the superclean limit is expected to be reached [16].

The flux-flow resistivity has been used in other superconductors to evaluate the coherence length ξ . However, IBS exhibit Pauli-limited upper critical fields [17], which flattens the temperature T dependence of $B_{c2}(T)$ by decreasing T . This property makes difficult the determination of ξ , which instead is related to the so-called orbital upper critical field $B_{c2}^{orb} = \Phi_0/(2\pi\xi^2)$. The evaluation of ξ is made even more complex by the multiple superconducting order parameters coexisting in IBS.

The framework for the correct determination of the main superconducting parameters from ρ_{ff} is then rather complicated in IBS, since all the peculiar

elements of their electronic structure must be taken into account. In this work we study the microwave flux flow resistivity of $\text{FeSe}_x\text{Te}_{1-x}$ epitaxial films to (i) assess whether the multiband superconductivity manifests in the $\rho_{ff}(B)$ dependence, differently from what observed in single crystals [13], (ii) shed light on the B_{c2}^{orb} temperature dependence, and (iii) explore the degree of quantization of bound levels in the vortex cores exhibited by this IBS.

The paper is structured as follows: Section 2 introduces the microwave techniques, the relevant models for the surface impedance and vortex motion resistivity, the samples preparation and properties. Section 3 will present the main results and discussions. Conclusions are presented in Section 4. Some details on data analysis are reported in the Appendix A.

2. Experiment and technique

2.1. Microwave Technique and Models

We use a microwave technique to measure the surface impedance $Z_s = E_{\parallel}/H_{\parallel}$ of $\text{Fe}(\text{Se},\text{Te})$ thin films. Here, E_{\parallel} and H_{\parallel} are the microwave electric and magnetic field, respectively, parallel to the sample surface. Z_s is the response function at microwave frequencies. Measurements are performed by means of a cylindrical dual mode dielectric-loaded resonator with the so-called surface perturbation technique [18]. A circular part of the sample surface is exposed to the resonator e.m. fields by means of a hole (diameter $\varnothing \approx 6$ mm) in a thin metal mask that partially covers it and holds it in a centered position (see Fig. 1). The

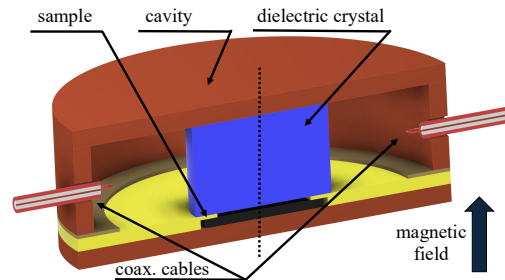


Figure 1. Dielectric loaded resonator used in the surface perturbation approach. The superconducting sample is depicted in black, the thin metal mask in yellow.

two resonant modes used in the measurements are the TE_{011} and TE_{021} , with resonant frequencies $\nu_{0,1} = 16.4$ GHz and $\nu_{0,2} = 26.6$ GHz respectively, thus well below the lowest gap energy exhibited by $\text{FeSe}_x\text{Te}_{1-x}$ (~ 2 meV $\simeq 480$ GHz [19]) so that no pair breaking can be induced by the microwave probe apart from very close to T_c . Both modes induce planar circular currents on the sample surface. The resonator is operated in transmission and its complex two-

port scattering coefficients $S_{ij}(\nu)$ are measured against frequency ν through a Vector Network Analyzer. With proper calibration and fitting procedures the resonant modes quality factors Q_i and resonant frequencies $\nu_{0,i}$ ($i = 1, 2$) are extracted [20]. From the magnetic field induced variations on Q_i and $\nu_{0,i}$ ($i = 1, 1$) at fixed temperature T , the corresponding variations on $\Delta Z_s(H; T)$ are determined:

$$\Delta Z_s(H) = Z_s(H) - Z_s(0) \quad (1a)$$

$$\Delta R_s(H) = G_{s,i} \left(\frac{1}{Q_i(H)} - \frac{1}{Q_i(0)} \right) \quad (1b)$$

$$\Delta X_s(H) = -2G_{s,i} \frac{\nu_{0,i}(H) - \nu_{0,i}(0)}{\nu_{0,i}(0)} \quad (1c)$$

where

$$Z_s(H) = R_s(H) + iX_s(H) \quad (2)$$

and $R_s = \text{Re}(Z_s)$ and $X_s = \text{Im}(Z_s)$ are the surface resistance and reactance, respectively, and $G_{s,i} = 1334 \Omega, 7455 \Omega$ are geometrical factors specific of each resonant mode, and they are determined through electromagnetic (e.m.) numerical simulation of the resonant structure. When measuring temperature induced variations $\Delta Z_s(T; H)$, an expression similar to Eq. (1) holds, with the addition of a temperature dependent background term which needs to be properly taken into account [18]. Since the e.m. field penetration depth has the London penetration depth λ as lower limit, and $\lambda(H = 0; T = 0) \simeq 500 \text{ nm}$ in FeSeTe compounds [13] is larger than the film thickness d , the e.m. field propagates through the film, reaches the substrate and yields a surface impedance in the so-called thin film regime [21]:

$$Z_s \simeq Z_{film} = \frac{\tilde{\rho}}{d}, \quad (3)$$

which is directly proportional to the sample complex resistivity $\tilde{\rho}$. In the mixed state the latter is given by the Coffey-Clem model [22]:

$$\tilde{\rho} = \frac{\rho_{vm} + i/\sigma_2}{1 + i\sigma_1/\sigma_2} \simeq \rho_{vm} + i\frac{1}{\sigma_2} = \rho_{vm} + i2\pi\nu\mu_0\lambda^2 \quad (4)$$

The two fluid conductivity $\sigma_{2f} = \sigma_1 - i\sigma_2$ incorporates the quasi-particle contribution σ_1 and the superfluid contribution $\sigma_2 = 1/(2\pi\nu\mu_0\lambda^2)$. The approximate equality in Eq. (4) holds far from the $B_{c2}(T)$ line, where $\sigma_1 \ll \sigma_2$. The vortex motion resistivity is a complex, frequency dependent quantity which, on very general grounds [23], can be cast in the following form:

$$\rho_{vm}(B) = \rho_{vm,R} + i\rho_{vm,X} = \rho_{ff} \frac{\chi + i\nu/\nu_c}{1 + i\nu/\nu_c} \quad (5)$$

where the vortex parameters ρ_{ff} , ν_c and χ are the flux flow resistivity, characteristic frequency and thermal

creep factor, respectively. With the measurement of $\rho_{vm}(B; \nu)$ at the two operating frequencies $\nu_{0,i}$, Eq. (5) yields four observables (real and imaginary parts at two frequencies) which can be used to extract the field dependent vortex parameters through analytical inversion of the equations, as done here following Ref. [24], or through fitting procedures [25]. In this way the flux flow resistivity can be determined independently from pinning contributions, in contrast with what happens, for example, in dc magnetoresistivity measurements where flux flow and pinning effects are intermingled in the measured dc resistivity ρ_{dc} . It is worth noting that, since $\rho_{vm}(B = 0) = 0$, when pair-breaking effects [26] are negligible so that λ is independent from B , field-induced variations on Z_s in the thin film regime directly yields $\rho_{vm}(B)$:

$$\Delta Z_s(B) = \frac{\rho_{vm}(B)}{d} \quad (6)$$

2.2. Samples preparation

The samples under study are $\text{FeSe}_x\text{Te}_{1-x}$ of nominal composition $x = 0.5$ and were deposited by Pulsed Laser Deposition on CaF_2 substrates, $7 \times 7 \text{ mm}^2$ and 0.5 mm thick. The deposition was carried out in a high vacuum PLD system equipped with a Nd:YAG laser at 1024 nm , using a $\text{FeSe}_{0.5}\text{Te}_{0.5}$ target synthesized with a two-step method [27]. The laser parameters were optimized to obtain high quality epitaxial thin films: 3 Hz repetition rate, 2 J/cm^2 laser fluency (2 mm^2 spot size) and a 5 cm substrate-target distance [28]. During the deposition, the substrate was kept at 350°C at the base pressure of the system ($1 \times 10^{-8} \text{ mbar}$). Superconducting transitions R_s vs T measured at $\nu_{0,2} = 27 \text{ GHz}$ and at zero field are reported in Fig. 2, whence the (onset) T_c , the normal state resistance R_n and the normal state resistivity $\rho_n = R_n d$ as derived from microwave measurements, see Eq.(3). Films have been grown by Laser ablation. The thickness has been calibrated against deposition time. Thus, a systematic uncertainty $\pm 10\%$ on the thickness of each sample with respect to the nominal value is estimated. Sample data are reported in Table 1, where it can be seen that they exhibit normal state resistivity and T_c in good agreement with other similar samples [27, 29].

Sample	thickness d (nm)	T_c (K)	R_n (Ω)	ρ_n ($\Omega \cdot \text{m}$)
FST#1	240	18.0	13.0	3.1×10^{-6}
FST#2	400	18.6	7.5	3.0×10^{-6}

Table 1. Studied samples with main parameters. The (onset) critical temperature T_c is determined from the superconducting transition on R_s as reported in Fig. 2.

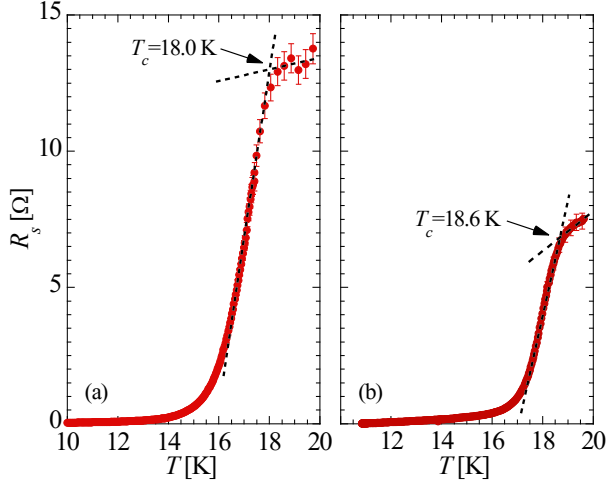


Figure 2. Superconducting transitions R_s vs T at $\nu_{0,2} = 27$ GHz and at zero field. (a) Sample FST#1; (b) sample FST#2.

3. Results

3.1. The flux flow resistivity

Field induced variations of the surface impedance, $\Delta Z_s(H)$, have been measured as a function of the static magnetic field in the range $H \in [0 \text{ T}, 1.2 \text{ T}]$. The field was applied perpendicularly to the sample surface, that is parallel to the crystallographic c -axis of the samples. Raw measurements performed at the two measuring frequencies $\nu_{0,1} = 16$ GHz and $\nu_{0,2} = 27$ GHz are fully reported in the Appendix A.

We are here focussed on the flux-flow resistivity. To derive ρ_{ff} we note that at the low magnetic fields here applied, no significant pair breaking is expected unless very close to T_c (see the Appendix A for a quantitative assessment). In this case, since the sample is fully in the thin film regime [21], one directly obtains the vortex motion resistivity as $\rho_{vm} = \Delta Z_s(H)d$, see Eq. (6)

The so-obtained flux flow resistivity ρ_{ff} vs H is reported in Fig. 3 for selected temperatures in both samples studied. A first significant feature is the slight downward curvature. Although extrinsic effects could come into play (e.g., in Nb_3Sn coatings because of the interaction of vortices with very large grains [30]), a downward curvature in ρ_{ff} is typically an indication of multiband superconductivity, as exhibited by MgB_2 [31, 2, 32, 33] and several IBS superconductors [5, 6, 9]. A second signature of multiband superconductivity resides in the initial slope α of the normalized ρ_{ff}/ρ_n vs the normalized applied B/B_{c2} , defined e.g. by:

$$\rho_{ff} = \rho_n \alpha \frac{B}{\Phi_0 / (2\pi\xi^2)} \text{ for } B/B_{c2} \ll 1 \quad (7)$$

where ξ is the coherence length and Φ_0 is the flux

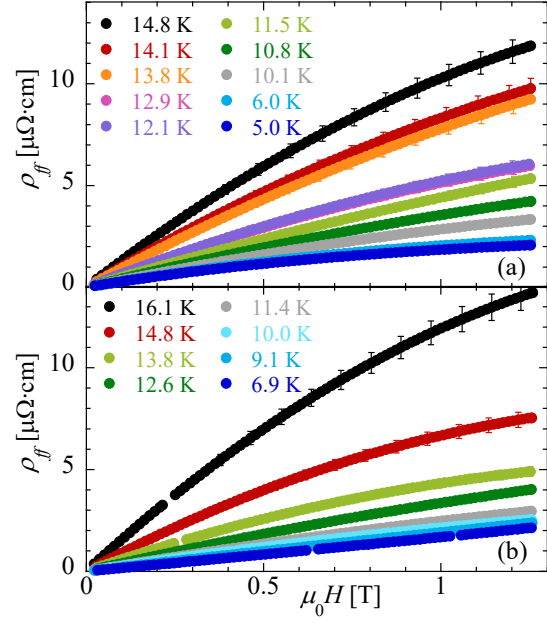


Figure 3. Flux flow resistivity ρ_{ff} vs H , at selected T . (a) sample FST#1; (b) sample FST#2.

quantum. α is linked to the microscopic details of the current patterns in and around the moving vortices, the quasi-particle (QP) scattering times and density, the actual energy levels available in the vortex cores, the anisotropy of the Fermi Surface (FS) and the single/multiband nature of the superconductor [11, 34, 12, 35, 14, 36]. In various limits and specific conditions:

- $\alpha = 1$ for the well-known Bardeen-Stephen (BS) model [10], here fluxons are modeled as cylindrical normal regions of radius ξ where normal currents flow and dissipate. In this case, Eq.(7) holds up to B_{c2} ;
- $\alpha = [\Phi_0/c][1 + \beta_A(2\kappa^2 - 1)][\kappa\rho_n\tau]^{-1} \simeq 0.4 < 1$ for single band superconductors with paramagnetic impurities in gapless conditions, according to Time Dependent Ginzburg-Landau (TDGL) theory [11, 12], being κ the GL parameter [26] and $\beta_A \approx 1.16$ the Abrikosov's parameter for triangular flux line lattice;
- $\alpha \approx \frac{\Delta_0^2}{\langle \Delta^2 \rangle_{\text{FS}}} > 1$ in single band superconductors with anisotropic Fermi Surface (FS), being $\langle \rangle_{\text{FS}}$ the angular average over the FS and Δ_0 the maximum value of the gap over the FS. For superconductors with a nodal gap like the cuprates, $\alpha \approx 2$ [37];
- $\alpha \geq 1$ in multiband superconductors where one band is more sensitive to the magnetic field (oversimplifying, with an upper critical field smaller in one band with respect to others) [13]. In this situation a steep B dependence appears

in ρ_{ff} , as observed in MgB_2 and in several IBS. Theoretically, the B slope is obtained by modeling the multiband superconductors as in [2], with $\rho_{ff}^{-1} = \sum_k \rho_{ffk}^{-1}$, with k running over the contributing bands.

α is than an essential parameter to study the microscopic nature of a superconductor. To compute α from ρ_{ff} an estimate of ξ entering Eq. (7) is needed. The coherence length is usually obtained in terms of the orbital upper critical field, $B_{c2}^{orb} = \Phi_0/(2\pi\xi^2)$ [38]. A direct measure of B_{c2}^{orb} in IBS is difficult: in fact, it is well known that IBS, and $\text{FeSe}_x\text{Te}_{1-x}$ in particular, can have a strongly Pauli limited $B_{c2} \ll B_{c2}^{orb}$ [17, 39], in particular at low T , so that B_{c2} typically steeply rises near T_c and then flattens as $T \rightarrow 0$. A preliminary estimation of B_{c2}^{orb} can be done following the WHH [40, 41] formula for single band SC, which reads $H_{c2}^{orb}(T=0) = -0.69H'_{c2}T_c$, where $H'_{c2} = dH_{c2}(T)/dT|_{T_c}$. In this case, one relies on measurements taken close to T_c , where the upper critical field is not Pauli-limited, to extrapolate the values at low T . Using this approach, dc resistivity measurements gave high values of B_{c2}^{orb} , whence an estimation of the ab -plane $\xi = (\phi_0/(2\pi B_{c2}^{orb}))^{1/2} \approx 1 \text{ nm}$ [17], typical of the clean limit. We discuss this aspect on our samples later on, in Subsection 3.3. It must however be remarked that the values of H'_{c2} vary significantly with the sample growth. In a $\text{FeSe}_x\text{Te}_{1-x}$ crystal, $H'_{c2} \approx -5.5 \text{ T/K}$ was obtained from dc resistivity measurements, together with $\alpha < 1$ which was explained in terms of important scattering by magnetic impurities, presumably due to an excess of Fe [13]. Also other single crystals [42, 43, 44] yields different H'_{c2} with respect to epitaxial thin films, among which H'_{c2} was observed to be dependent on the substrate [39, 45, 46, 47], being CaF_2 the substrate that provided the highest values [48]. Thus, further data analysis cannot be grounded on data coming from very different samples.

3.2. Orbital upper critical field

We now evaluate $B_{c2}^{orb}(T)$ in the present samples. First, we take advantage of measurements of the derivative $H'_{c2} = dH_{c2}(T)/dT|_{T_c}$ performed on $\text{Fe}(\text{Se},\text{Te})$ epitaxial thin films grown in the same laboratory and with the same technique and substrate as for our samples, which is an essential point for a reliable analysis. Ref. [45, 39, 46, 47] provide H'_{c2} equal to -30 T/K , -22 T/K , -25 T/K , -18 T/K , respectively. Although different samples grown by the same technique present sizable differences in H'_{c2} , despite the little difference in T_c , large values are always found. On average, we can take $H'_{c2} \approx -24 \text{ T/K}$. We then exploit the magnetic-field-scaling properties of ρ_{ff} : with negligible T dependence of α and ρ_n , its only T dependence comes

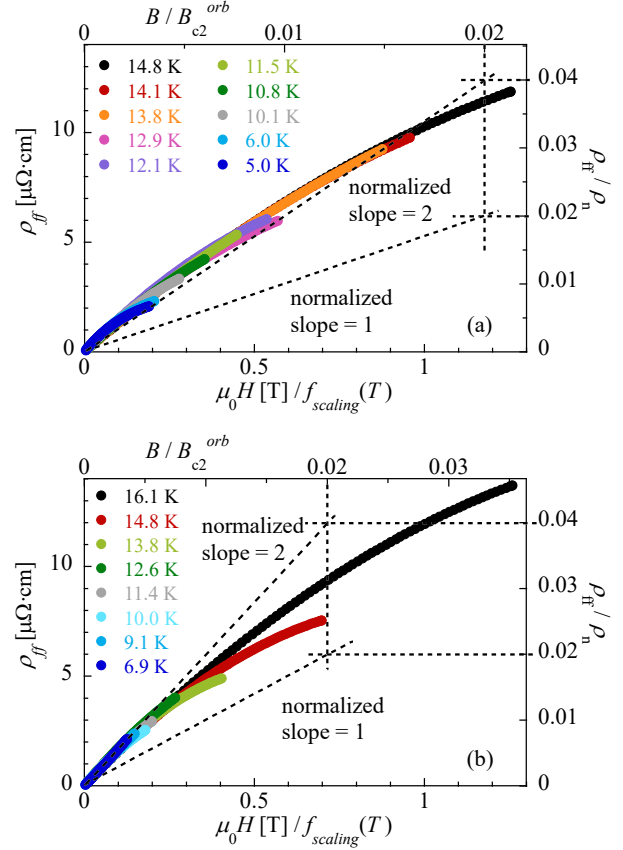


Figure 4. Scaling of the flux flow resistivity ρ_{ff} vs H . Right and up axes report the normalized quantities, which allow to extract the slope α . (a) sample FST#1; (b) sample FST#2.

from B_{c2}^{orb} so that $\rho_{ff}(B, T) = \rho_{ff}(B/B_{c2}^{orb}(T))$. Hence, a scaling function $f_{scaling}(T)$ can be determined so that the various experimental curves $\rho_{ff}(B/f_{scaling}(T))$ superimpose. Such scaling is satisfactory, in particular at low fields, as reported in Fig. 4 for both samples. The so-obtained $f_{scaling}(T)$ directly yields the temperature dependence of $B_{c2}^{orb}(T)$ apart from an overall scale factor only. To obtain absolute $B_{c2}^{orb}(T)$, we assume the numerical value $|H'_{c2}| = 24 \text{ T/K}$ presented above.

The corresponding $B_{c2}^{orb}(T)$ is reported in Fig. 5. As it can be seen, both samples present the same values of B_{c2}^{orb} , with a temperature dependence which reminds closely the behaviour of other multiband superconductors: see e.g. the indication of a change of curvature at $t \approx 0.65$. Figure 5 is the first of the results of this paper: the measurement of the flux-flow resistivity allows for the determination of the orbital upper critical field in these Pauli-limited superconductors.

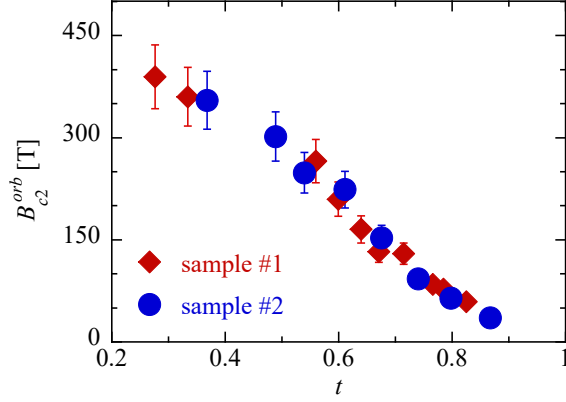


Figure 5. Estimated B_{c2}^{orb} vs $t = T/T_c$ for both samples. The B_{c2}^{orb} vs t dependence is identical.

3.3. Quasiparticle scattering time in the vortex cores: moderately clean regime

Once B_{c2}^{orb} is obtained, the normalized plots ρ_{ff}/ρ_n vs B/B_{c2}^{orb} in Fig. 4 allow for further considerations. Subsequent analysis must take into account that we obtain $\alpha \geq 2$, a clear confirmation of multiband physics. The obtained result places the thin $\text{FeSe}_x\text{Te}_{1-x}$ films here studied together with the majority of the other IBS, which predominantly exhibit $\alpha > 1$ [5, 6, 7, 8, 9], and it complicates the elaboration of ρ_{ff} .

In fact, ρ_{ff} can be used to determine the degree of cleanness since it allows for the determination of the quasiparticle scattering time τ_{core} in the vortex cores [14]. Let ΔE be the energy separation between the quantized bound levels in vortex cores [34] and $\delta E \approx \hbar/\tau_{core}$ their width due to scattering processes. The ratio $\Delta E/\delta E$ is a measure of the vortex core cleanness: if $\Delta E/\delta E \ll 1$ (dirty regime), the spread of the quantized levels let them overlap yielding a continuous levels spectrum, whereas $\Delta E/\delta E \gg 1$ yields the superclean regime. The in-between situation $\Delta E/\delta E \sim 1$ marks the so-called moderately clean regime.

Since:

- $\Delta E/\delta E \approx \omega_c \tau_{core}$ [34, 49], being ω_c the cyclotron angular frequency [14];
- $\langle \omega_c \tau_{core} \rangle_{\text{bands}} = \eta_{eff}/(\pi \hbar n)$, with $\eta_{eff} = \Phi_0 B/\rho_{ff}$ the effective vortex viscosity as measured in high frequency experiments with externally imposed (microwave) transport current density [14] and n the charge carrier density; $\langle \rangle_{\text{bands}}$ highlights that the quantity obtained from the vortex viscosity is averaged over the Fermi surfaces of all the bands possibly present;

the flux flow resistivity ρ_{ff} provides the needed window

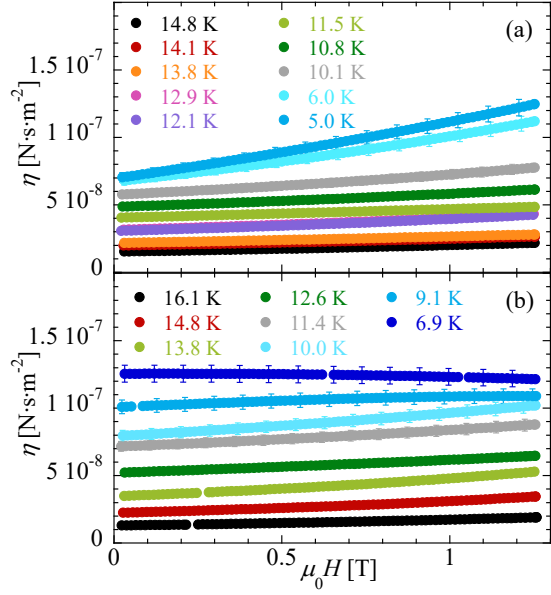


Figure 6. Effective vortex viscosity vs H at selected T . (a) sample FST#1; (b) sample FST#2.

into the vortex cores states to assess the degree of cleanness of the system.

The specific multibands of $\text{FeSe}_x\text{Te}_{1-x}$ must be considered. First, both hole and electron bands are present [19], with charge carrier density $n_h = 3.5 \times 10^{26} \text{ m}^{-3}$ and $n_e = 2.5 \times 10^{26} \text{ m}^{-3}$, for hole and electrons respectively, as determined through Hall measurements in $\text{FeSe}_{0.6}\text{Te}_{0.4}$ thin films of similar compositions to ours [50]. An average charge carrier density $n = 3.0 \times 10^{26} \text{ m}^{-3}$ can thus be used.

Second, since the bands have charge carriers of opposite signs, $\langle \omega_c \tau_{core} \rangle_{\text{bands}}$ undergoes a partial cancellation of the hole and electron contributions analogous to what can happen in Hall resistivity phenomena. An expression has been worked out in Ref. [15] highlighting this feature:

$$\langle \omega_c \tau_{core} \rangle_{\text{bands}} = \left| \frac{k_h(\omega_c \tau_{core})_h}{1 + (\omega_c \tau_{core})_h^2} - \frac{k_e(\omega_c \tau_{core})_e}{1 + (\omega_c \tau_{core})_e^2} \right| \quad (8)$$

where it can be assumed $k_h \approx k_e \approx 1$ [15]. Eq. (8) describes therefore the possible degree of quantization exhibited by the two bands.

Vortex viscosity data are reported in Fig. 6. It can be seen that the vortex viscosity has not a strong B dependence (which corresponds to the weak downward curvature of $\rho_{ff}(B)$), indicating that in the present field range $< 1.2 \text{ T}$ the scattering rate is only weakly field dependent. This fact does not exclude that, reaching the upper critical field, scattering could increase, thus potentially providing increased interband scattering. The obtained $\langle \omega_c \tau_{core} \rangle_{\text{bands}}$ vs T , at $B = 1.0 \text{ T}$, reported in Fig. 7 for the two samples, places the samples in the moderately clean

regime, with values $\langle\omega_c\tau_{core}\rangle_{\text{bands}} \simeq 0.5 - 1$ not far from those (1.0(5)) determined in FeSe [16]. The found value points presumably to the moderately clean regime for both bands since, according to [15], $\langle\omega_c\tau_{core}\rangle_{\text{bands}} \simeq 0.5 - 1$ reasonably correspond to similar, or even larger, individual values for the two bands.

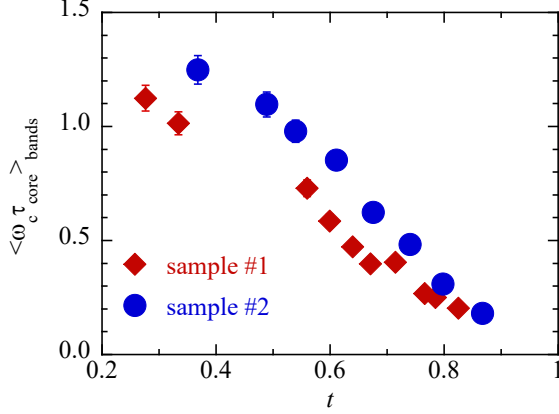


Figure 7. Effective normalized vortex core scattering time, $\langle\omega_c\tau_{core}\rangle_{\text{bands}}$ vs T in $\text{FeSe}_x\text{Te}_{1-x}$ for samples FST#1 and FST#2. The data show that both samples are in the moderately clean regime, reasonably for both the hole and electron bands. Data calculated for $\mu_0 H = 1.0$ T.

4. Conclusions

We have used a dual-frequency microwave technique to measure the flux-flow resistivity ρ_{ff} in epitaxial $\text{FeSe}_x\text{Te}_{1-x}$ thin films with nominal composition $x = 0.5$, grown on CaF_2 .

We have exploited the properties of the flux flow resistivity related to the quasiparticle excitations in the vortex cores to investigate the quasiparticle physics of $\text{FeSe}_x\text{Te}_{1-x}$.

We have shown that ρ_{ff} presents clear signatures of multiband superconductivity: namely, the ρ_{ff} slope vs the applied field B is $\alpha \geq 2$, a value typical of multiband superconductors.

The scaling analysis of $\rho_{ff}(B)$ against temperature allowed to estimate the temperature dependence of the orbital upper critical field B_{c2}^{orb} , a quantity otherwise inaccessible since B_{c2} is heavily influenced by Pauli limiting phenomena in IBS.

Moreover, by extracting the vortex core QP scattering times, and taking into account the hole and electron nature of QP, we have assessed that the samples under investigation are in the moderately clean regime. This further enforces the consistency of the observed multiband behaviour of $\rho_{ff}(B)$ slope, since it implies that intraband scattering should be not so large as to wash out the individuality of the various bands.

Acknowledgments

This work was partially supported by MIUR-PRIN Project “HIBISCUS” Grant 201785KWLE, MIUR-PRIN Project IronMOON Grant No. 2022BPJL2L, and INFN-CSN5 “SuperMAD”.

Appendix A.

Selected data for the measurements of the field-induced surface impedance shift are reported in Figs A1 and A2. The magnetic field is applied perpendicular to the sample surface (see also Fig. 1). From the data it is

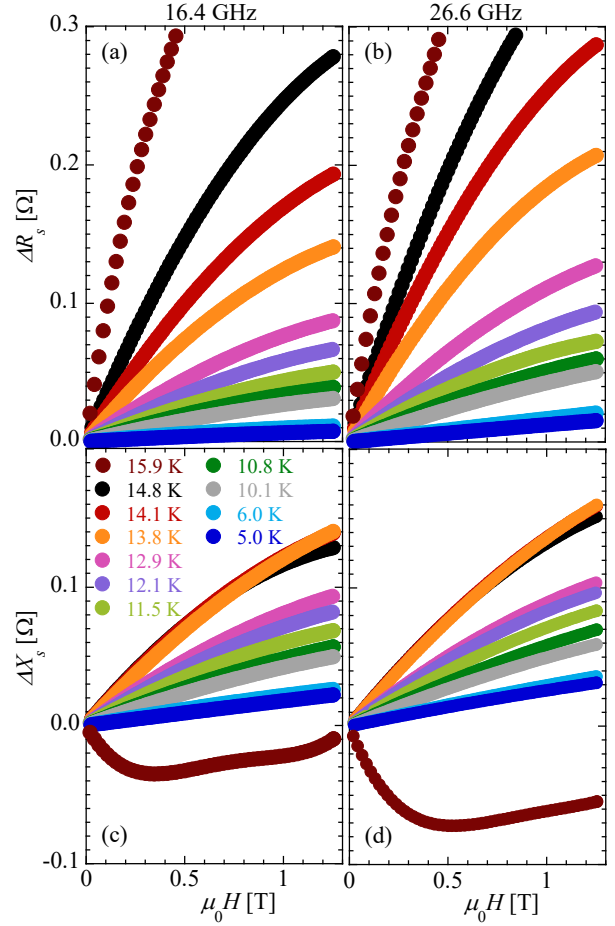


Figure A1. Measured $\Delta Z_s(H)$ for TE_{011} mode at 16.4 GHz and TE_{012} mode at 26.6 GHz, at selected T . The measurements are taken with $\mathbf{H} \perp$ sample surface. Data for sample FST#1. Error bars are within symbol size.

already possible to assess whether in Equation (4) the superfluid term can be treated as field-independent, that is the field-induced pair breaking is negligible at least at the moderate fields here applied. In fact, the signature of significant pair breaking is given by $\Delta X(H) < 0$ in the thin film limit, see Eq.(3): while at $H = 0$, $\text{Im}[\bar{\rho}] \neq 0$, at the superconducting transition it must become zero. The precise field dependence is

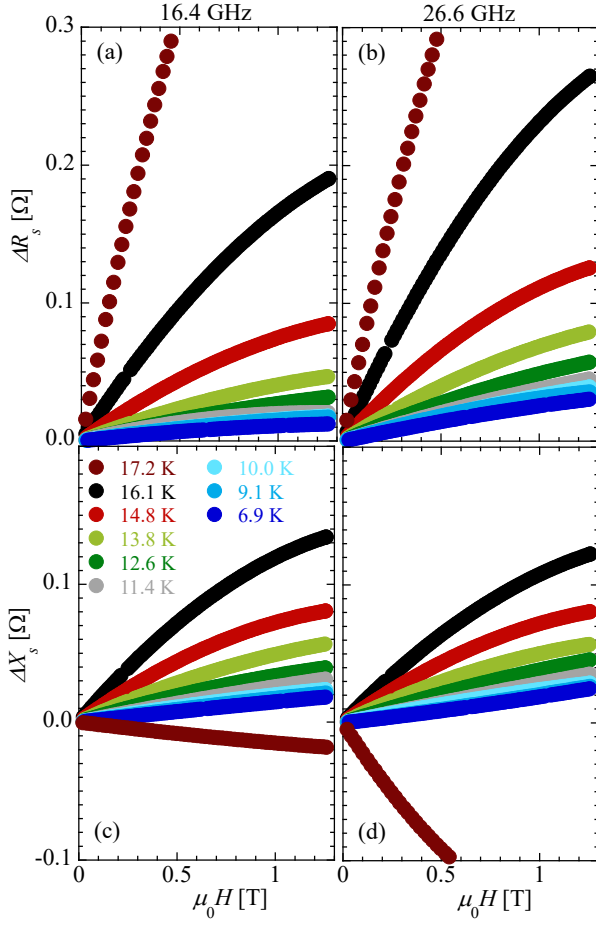


Figure A2. Measured $\Delta Z_s(H)$ for TE_{011} mode at 16.4 GHz and TE_{012} mode at 26.6 GHz, at selected T . The measurements are taken with $\mathbf{H} \perp$ sample surface. Data for sample FST#2. Error bars are within symbol size.

determined by the competition of pair breaking with all the possible details of pinning weakening, but it can be safely stated that when $\text{Im}[\Delta\tilde{\rho}(H)] \leq 0$, field-induced pairbreaking gives a relevant contribution to the response. In this case, Eq.(6) does not hold and the extraction of the vortex motion parameters is either much more complex or impossible. On the basis of this consideration, the observation of our data for $\Delta Z(H)$ brings to exclude from the analysis of the flux-flow resistivity ρ_{ff} the data at temperatures $T_1 > 14.8$ K in sample FST#1 and $T_2 > 16.1$ K in sample FST#2.

In the temperature range as determined above, we obtain from Eq.(6) the vortex motion resistivity as $\rho_{vm} = \Delta Z_s(H)d$. Since the uncertainty on the thickness d (10%) is the same for all T , it does not contribute to the scaling procedure described in Sec. 3, and the derived α and B_{c2}^{orb} (Subsections 3.1, 3.2) are not affected. The systematic uncertainty on d enters as a common scale factor only, on ρ_{ff} and η , which does not change the conclusions drawn in Subsection 3.3 for the analysis and thus it is not reported for

this quantity. In this paper, the figures report error bars corresponding to standard uncertainties with confidence interval 1.

- [1] Hosono H and Kuroki K 2015 *Physica C: Superconductivity and its Applications* **514** 399–422
- [2] Goryo J and Matsukawa H 2005 *J. Phys. Soc. Jpn.* **74** 1394–1396
- [3] Lin S Z and Bulaevskii L N 2013 *Phys. Rev. Lett.* **110** 87003
- [4] Sarti S, Amabile C, Silva E, Giura M, Fastampa R, Ferdeghini C, Ferrando V and Tarantini C 2005 *Phys. Rev. B* **72** 024542
- [5] Takahashi H, Okada T, Imai Y, Kitagawa K, Matsubayashi K, Uwatoko Y and Maeda A 2012 *Phys. Rev. B* **86** 144525
- [6] Okada T, Takahashi H, Imai Y, Kitagawa K, Matsubayashi K, Uwatoko Y and Maeda A 2012 *Phys. Rev. B* **86** 064516
- [7] Okada T, Takahashi H, Imai Y, Kitagawa K, Matsubayashi K, Uwatoko Y and Maeda A 2013 *Phys. C Supercond. its Appl.* **494** 109–112
- [8] Okada T, Takahashi H, Imai Y, Kitagawa K, Matsubayashi K, Uwatoko Y and Maeda A 2013 *Physica C: Superconductivity* **484** 27–30
- [9] Okada T, Imai Y, Takahashi H, Nakajima M, Iyo A, Eisaki H and Maeda A 2014 *Phys. C Supercond.* **504** 24–27
- [10] Bardeen J and Stephen M 1965 *Phys. Rev.* **140** 1197–1207
- [11] Schmid A 1966 *Phys kondens Materie* **5** 302–317
- [12] Larkin, AI and Ovchinnikov Y 1986 *Vortex Motion in Superconductors Nonequilibrium Supercond.* ed Langenberg, DN and Larkin A (Amsterdam: Elsevier) chap 11, pp 493–542
- [13] Okada T, Nabeshima F, Takahashi H, Imai Y and Maeda A 2015 *Phys. Rev. B* **91** 054510
- [14] Golosovsky M, Tsindlekht M and Davidov D 1996 *Supercond. Sci. Technol.* **9** 1–15
- [15] Ogawa R, Nabeshima F and Maeda A 2023 *J. Phys. Soc. Jpn.* **92** 064707
- [16] Okada T, Imai Y, Urata T, Tanabe Y, Tanigaki K and Maeda A 2021 *J. Phys. Soc. Jpn.* **90** 094704
- [17] Tarantini C, Gurevich A, Jaroszynski J, Balakirev F, Bellingeri E, Pallecchi I, Ferdeghini C, Shen B, Wen H H and Larbalestier D C 2011 *Phys. Rev. B* **84** 184522
- [18] Alimenti A, Torokhtii K, Silva E and Pompeo N 2019 *Meas. Sci. Technol.* **30** 065601
- [19] Miao H, Richard P, Tanaka Y, Nakayama K, Qian T, Umezawa K, Sato T, Xu Y M, Shi Y B, Xu N, Wang X P, Zhang P, Yang H B, Xu Z J, Wen J S, Gu G D, Dai X, Hu J P, Takahashi T and Ding H 2012 *Phys. Rev. B* **85** 094506
- [20] Torokhtii K, Alimenti A, Pompeo N and Silva E 2020 *Acta IMEKO* **9** 47–52
- [21] Pompeo N, Alimenti A, Torokhtii K, García P V and Silva E 2025 *IEEE Transactions on Instrumentation and Measurement* **74** 1–15
- [22] Coffey M W and Clem J R 1991 *Phys. Rev. Lett.* **67** 386–389
- [23] Pompeo N, Silva E, Ausloos M and Cloots R 2008 *J. Appl. Phys.* **103** 103912
- [24] Pompeo N, Torokhtii K, Alimenti A and Silva E 2021 *Measurement* **184** 109937
- [25] Pompeo N et al., *Unpublished*
- [26] Tinkham M 1996 *Introduction to Superconductivity* 2nd ed (New York, NY, USA: McGraw-Hill, Inc.) ISBN 0-07-06878-6
- [27] Palenzona A, Sala A, Bernini C, Braccini V, Cimperle M R, Ferdeghini C, Lamura G, Martinelli A, Pallecchi I, Romano G, Tropeano M, Fittipaldi R, Vecchione A, Polyanskii A, Kametani F and Putti M 2012 *Supercond. Sci. Technol.* **25** 115018
- [28] Sylva G, Bellingeri E, Ferdeghini C, Martinelli A, Pallecchi I, Pellegrino L, Putti M, Ghigo G, Gozzelino L, Torsello D, Grimaldi G, Leo A, Nigro A and Braccini V 2018 *Supercond. Sci. Technol.* **31** 54001
- [29] Pompeo N, Alimenti A, Torokhtii K, Sylva G, Braccini V and Silva E 2020 *J. Phys. Conf. Ser.* **1559** 012055
- [30] Vidal García P et al., *Unpublished, to be presented at European Conference on Applied Superconductivity 2025*
- [31] Shibata A, Matsumoto M, Izawa K, Matsuda Y, Lee S and Tajima S 2003 *Phys. Rev. B* **68** 060501(R)
- [32] Alimenti A, Torokhtii K, Vidal García P, Silva E, Grigoroscuta M A, Badica P, Crisan A and Pompeo N 2023 *Materials* **16** 205
- [33] Alimenti A, Silva E, Torokhtii K, García P V, Badica P, Crisan A, Grigoroscuta M A and Pompeo N 2025 *Superconductivity* 100170
- [34] Caroli C, De Gennes P G and Matricon J 1964 *Phys. Lett.* **9** 307–309
- [35] Dorsey A T 1992 *Phys. Rev. B* **46** 8376–8392
- [36] Kopnin N and Volovik G 1997 *Phys. Rev. Lett.* **79** 1377–1380
- [37] Matsuda Y, Shibata A, Izawa K, Ikuta H, Hasegawa M and Kato Y 2002 *Phys. Rev. B* **66** 014527–1/014527–8
- [38] Kopnin N 2001 *Theory of Nonequilibrium Superconductivity* (Oxford: Clarendon Press) ISBN 978-0-19-850788-8
- [39] Grimaldi G, Leo A, Martucciello N, Braccini V, Bellingeri E, Ferdeghini C, Galluzzi A, Polichetti M, Nigro A, Villegier J C and Pace S 2019 *IEEE Trans. Appl. Supercond.* **29** 7500104
- [40] Werthamer N R, Helfand E and Hohenberg P C 1966 *Phys. Rev.* **147** 295–302
- [41] Khim S, Kim J W, Choi E S, Bang Y, Nohara M, Takagi H and Kim K H 2010 *Physical Review B* **81** 184511
- [42] Leo A, Guarino A, Grimaldi G, Nigro A, Pace S, Bellingeri E, Kawale S, Ferdeghini C and Giannini E 2014 *J. Phys. Conf. Ser.* **507** 12029
- [43] Galluzzi A, Buchkov K, Tomov V, Nazarova E, Leo A, Grimaldi G, Nigro A, Pace S and Polichetti M 2017 *Supercond. Sci. Technol.* **31** 015014
- [44] Galluzzi A, Buchkov K, Tomov V, Nazarova E, Kovacheva D, Leo A, Grimaldi G, Pace S and Polichetti M 2018 *Journal of Applied Physics* **123** 233904
- [45] Bellingeri E, Kawale S, Cagliaris F, Braccini V, Lamura G, Pellegrino L, Sala A, Putti M, Ferdeghini C, Jost A, Zeitler U, Tarantini C and Jaroszynski J 2014 *Supercond. Sci. Technol.* **27** 044007
- [46] Leo A, Sylva G, Braccini V, Bellingeri E, Martinelli A, Pallecchi I, Ferdeghini C, Pellegrino L, Putti M, Ghigo G, Gozzelino L, Torsello D, Pace S, Nigro A and Grimaldi G 2019 *IEEE Trans. Appl. Supercond.* **29** 7300205
- [47] Leo A, Nigro A, Braccini V, Sylva G, Provino A, Galluzzi A, Polichetti M, Ferdeghini C, Putti M and Grimaldi G 2020 *Supercond. Sci. Technol.* **33** 104005
- [48] Kawale S, Bellingeri E, Braccini V, Pallecchi I, Putti M, Grimaldi G, Leo A, Guarino A, Nigro A and Ferdeghini C 2013 *IEEE Trans. Appl. Supercond.* **12** 7500704
- [49] Blatter G, Feigel'man M, Geshkenbein V, Larkin A and Vinokur V 1994 *Rev. Mod. Phys.* **66** 1125–1388
- [50] Nabeshima F, Ishikawa T, Shikama N and Maeda A 2020 *Phys. Rev. B* **101** 184517